

Degradation-Noise-Aware Deep Unfolding Transformer for Hyperspectral Image Denoising

Haijin Zeng
haijin.zeng@imec.be
IMEC-UGent
Ghent, Belgium

Jiezhong Cao
jiezhong.cao@vision.ee.ethz.ch
Computer Vision Lab, ETH
Zurich, Switzerland

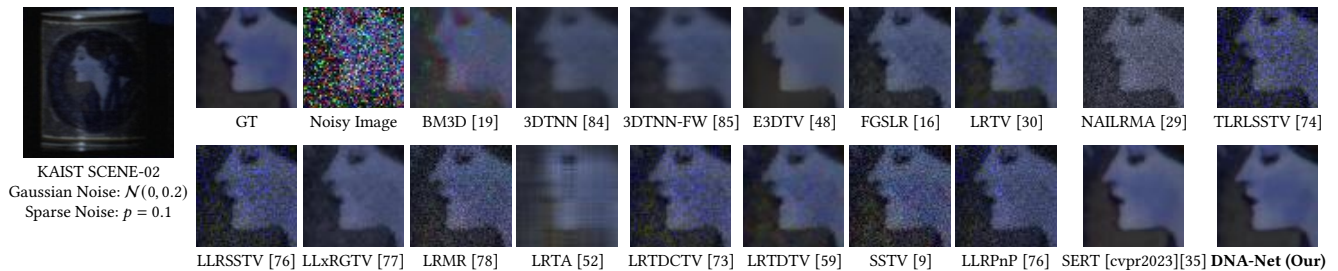
Kai Feng
fengkainpu@gmail.com
NPU
Xi'an, China

Shaoguang Huang
CUG
Wuhan, China

Hongyan Zhang
CUG
Wuhan, China

Hiep Luong
IMEC-UGent
Ghent, Belgium

Wilfried Philips
IMEC-UGent
Ghent, Belgium



ABSTRACT

Hyperspectral imaging (HI) has emerged as a powerful tool in diverse fields such as medical diagnosis, industrial inspection, and agriculture, owing to its ability to detect subtle differences in physical properties through high spectral resolution. However, hyperspectral images (HSIs) are often quite noisy because of narrow band spectral filtering. To reduce the noise in HSI data cubes, both model-driven and learning-based denoising algorithms have been proposed. However, model-based approaches rely on hand-crafted priors and hyperparameters, while learning-based methods are incapable of estimating the inherent degradation patterns and noise distributions in the imaging procedure, which could inform supervised learning. Secondly, learning-based algorithms predominantly rely on CNN and fail to capture long-range dependencies, resulting in limited interpretability. This paper proposes a Degradation-Noise-Aware Unfolding Network (DNA-Net) that addresses these issues. Firstly, DNA-Net models sparse noise, Gaussian noise, and explicitly represent image prior using transformer. Then the model is unfolded into an end-to-end network, the hyperparameters within the model are estimated from the noisy HSI and degradation model and utilizes them to control each iteration. Additionally, we introduce a novel U-Shaped Local-Non-local-Spectral Transformer (U-LNSA) that captures spectral correlation, local contents, and non-local dependencies simultaneously. By integrating U-LNSA into DNA-Net, we present the first Transformer-based deep unfolding HSI denoising method. Experimental results show that DNA-Net outperforms state-of-the-art methods, and the modeling of noise distributions helps in cases with heavy noise.

KEYWORDS

Hyperspectral image, unfolding, denoising, transformer

1 INTRODUCTION

Hyperspectral image (HSI) comprises numerous bands that cover a broad spectrum range. Due to its ability to incorporate wavelengths beyond the visible spectrum and distinguish subtle differences in various materials, HSI offers significant advantages for various applications, including remote sensing, face recognition, medical diagnosis, and classification [37, 68, 70, 82]. However, current hyperspectral imaging techniques always produce HSIs with substantial degradation, e.g., electronic noise, quantization noise [35, 45, 87], which emphasizes the importance of robust denoising algorithms to improve the image quality of HSI.

Research on HSI denoising can be categorized into four major directions: model-based models, Plug-and-play (PnP) algorithms, End-to-end (E2E) deep neural networks, and Deep unfolding methods. **Model-based methods** for HSI reconstruction rely on hand-crafted image priors such as sparsity based total variation, and spectral correlation based low-rank representation, among others. These methods have theoretical foundations and can be explained. However, they require manual parameter adjustment and also need lots of iterations to be converged, which slows down the reconstruction process. **PnP algorithms** employ pre-trained denoising network as Plug-and-Play priors of traditional model-based methods. However, the performance of PnP methods is limited by the fixed nature of the pre-trained networks, which cannot be re-trained and the network is not customised for the task.

E2E approaches for HSI denoising usually use a convolutional neural network (CNN), to learn the mapping function from a noisy HSI to the clean HSI. E2E methods have the advantages of deep learning. Nevertheless, they disregard the degradation mechanism and noise distributions of HSI by learning a brute-force mapping from the noisy hyperspectral images to the underlying noise free HSI. Additionally, E2E methods lack theoretical foundations, interpretability.

Deep unfolding methods involve the utilization of a sequence of stages to map noisy HSI observations to clean HSI cubes. Typically, each stage incorporates a fidelity phase, followed by a single-stage network that learns the underlying denoiser prior [64, 66]. It presents a highly interpretable network architecture that explicitly characterizes both the image priors and degradation model. These methods offer a hybrid approach that combines the strengths of both deep learning and model-based techniques, leading to promising denoising performance. Nonetheless, current deep unfolding algorithms encounter two primary issues. Firstly, the iterative learning process in these methods is highly dependent on the degradation pattern of the hyperspectral image but current methods do not estimate the HSI degradation patterns and noise characteristics to adjust the denoising network in each iteration. Secondly, the existing deep unfolding methods predominantly employ CNNs, which exhibit limitations in capturing non-local self-similarity and long-range dependencies, both critical for HSI denoising.

Recently, the attention mechanism-based Transformer [57] model has emerged as a promising solution for overcoming the drawbacks of CNNs. The Transformer’s strong capability to model the interactions of global contexts or non-local spatial regions has resulted in its wide application in image processing. For instance, image classification [2, 39], object detection [69, 86], semantic segmentation [6, 63], human pose estimation [36, 67], image restoration [12, 22], *etc.* However, the use of Transformer in HSI denoising is faced with two primary issues. Firstly, the computational complexity of global Transformer [24] increases quadratically with spatial dimensions, making it unaffordable in some cases. Secondly, the receptive fields of local Transformer [39] are limited to position-specific windows, which hinders the matching of highly related content tokens during self-attention computation [5], and it also does not take into account the spectral correlation of HSI.

In this paper, we propose a novel approach to address the problem of HSI denoising by designing a Degradation-Noise-Aware Unfolding Network (DNA-Net) based on the maximum a posteriori (MAP) theory. Unlike previous deep unfolding methods, DNA-Net accurately models sparse noise and Gaussian noise using l_1 -norm and F-norm, respectively. Moreover, it adaptively estimates informative hyperparameters from degraded noisy observations. These hyperparameters are then fed into each iteration of DNA-Net to adaptively scale the noise reduction.

Additionally, a new U-shaped local-non-local-spectral Transformer (U-LNSA) is proposed as the sub-denoiser in each iteration. U-LNSA jointly extracts local contextual information, models non-local dependencies and spectral correlation of HSI, while being computationally efficient. To achieve this, a spatial-spectral-split Multi-head Self-Attention block is customized to compose the basic unit of U-LNSA. Specifically, LNSA has three parallel attention

branches, which calculate the self-attention within the local window, capture cross-window interactions by shuffling the tokens, and model the spectral information, respectively.

Finally, U-LNSA is integrated into DNA-Net to form an iterative architecture called the Degradation-Noise-Aware Unfolding Transformer. Experiments demonstrate that DNA-Net outperforms latest state-of-the-art (SOTA) methods by over 1.49dB, as illustrated in the teaser. Our contributions are summarized as follows:

- (1) We propose an MAP-based unfolding network for HSI denoising that accurately models the degradation pattern and noise distributions of HSI, while incorporating adaptive hyperparameter estimation.
- (2) We propose a novel Transformer U-LNSA and plug it into DNA-Net to do HSI denoising. To the best of our knowledge, DNA-Net is the first Transformer-based deep unfolding method for HSI denoising.
- (3) DNA-Net achieves significant performance improvements over state-of-the-art methods, particularly in scenarios involving heavy noise.

2 RELATED WORK

In recent years, a substantial body of research has been devoted to mitigating the challenge of denoising hyperspectral images. The literature on this topic can be broadly classified into two principal categories: conventional, which encompasses optimization-based models, and deep-learning-based approaches.

2.1 Optimization and PnP-based Methods

Optimization-based methods have been extensively employed for HSI denoising, with full-rank, low-rank matrix, and low-rank tensor approaches being the most commonly used techniques. Full-rank approaches utilize wavelet-based methods, combined with spatial and/or spectral handcrafted regularizers, to effectively capture the spatial and spectral dependencies of the HSI. On the other hand, low-rank approaches rely on low-rank constraints, such as the nuclear norm, to exploit the high spectral correlation or local smoothness present in the HSI. To sum up, traditional optimization-based methods formulate the problem as an optimization objective that takes into account the unique properties of the spectrum and images. Various handcrafted regularization terms, such as total variation, wavelet constraint, and low-rank representation [42, 44, 50, 54, 59, 61, 71, 83], have been incorporated in the optimization framework to enhance the denoising performance. These optimization-based methods are flexible enough to remove different types of noise [14, 31] and can be extended to tasks beyond denoising [11, 26, 27, 49]. However, the performance of these methods is limited by the degree of matching between the handcrafted regularization and the underlying properties of the HSI, especially for complex real scenes [14, 31]. To address this issue, plug-and-play methods integrate optimization-based methods with a learning-based prior [7, 21, 75, 88], such as a plug-and-play Gaussian denoiser, to handle complex noise types that cannot be easily modeled by handcrafted regularization [20, 80]. These methods can remove different types of noise and can also be extended to tasks beyond denoising, e.g., [38, 41, 41, 80].

2.2 CNN and Unfolding based Methods

Recently, several deep architectures have been proposed that take advantage of advances in deep learning for HSI denoising [3, 10, 13, 23, 25, 33, 34, 46, 53, 60, 62, 65, 72, 79]. In [72], a spatio-spectral deep residual CNN was proposed that utilizes 3D and 2D convolutional filters to capture the dependencies of the images. The MemNet [55] network and one variation MemNetRes [18] (which is a combination of MemNet with the Hyres approach [61]), can provide competitive hyperspectral denoising results. Inspired by the success of the 2D image denoising network DnCNN [79], Chang *et al.* [10] proposed HSI-DeNet, which learns multi-channel 2-D filters to model spectral correlation. Yuan *et al.* [72] introduced a residual network structure with a sliding window strategy for remote sensed HSI. To further exploit spatial-spectral correlation, Dong *et al.* [23] designed a 3D U-net architecture. Although these methods have been successfully applied to various HSIs, most of them are limited to exploring inter-spectral correlations, which are significantly important for HSI denoising. To address this issue, the 3D Quasi-Recurrent Neural Network (QRNN3D) [62] employs 3D convolution components and quasi-recurrent pooling functions to capture the spatio-spectral dependencies of the HSI. Li *et al.* [35] introduces a novel approach for HSI denoising, termed as Spectral Enhanced Rectangle Transformer (SERT). This method effectively leverages the non-local spatial similarity as well as the global spectral low-rank characteristic of noisy images, resulting in new SOTA denoising performance.

3 PROPOSED METHOD

3.1 Degradation Model of HSI

In HSI imaging system, we denote the observed 3D HSI and the latent noise free HSI as tensor $\mathcal{Y} \in \mathbb{R}^{M \times N \times P}$ and $\mathcal{X} \in \mathbb{R}^{M \times N \times P}$, respectively, where P is the total number of spectral bands, M, N denote the HSI's spatial height, width. Previous deep neural network based denoising approaches mainly focus on learning a deep blind model with paired training data, to reconstruct a hyperspectral image $\hat{\mathcal{X}}$ by referencing the observed noisy image \mathcal{Y} . Mathematically, deep blind model is equivalent to maximize a posterior (MAP):

$$\min_{\theta} \mathcal{L}(\hat{\mathcal{X}}(\mathcal{Y}, \theta), \mathcal{X}), \text{ s.t.}, \hat{\mathcal{X}} = \arg \min_{\hat{\mathcal{X}}} F(\hat{\mathcal{X}}, \mathcal{Y}) + \Phi(\hat{\mathcal{X}}), \quad (1)$$

where $F(\mathcal{X}, \mathcal{Y})$ denotes image fidelity term, $\Phi(\mathcal{X})$ is the regularization used to represent the prior of HSI, $\mathcal{L}(\cdot)$ denotes the loss function, θ is the learn-able parameters of network. However, they do not estimate the HSI degradation patterns or model noise characteristics to guide the learning phase.

HSI are typically degraded by various types of noise, including Gaussian noise, sparse noise (such as impulse noise and stripes), and Poissonian noise [30, 87]. Meanwhile, Poissonian noise has emerged as a major concern in real HSI due to the decrease in spectral bandwidth resulting from an increase in the number of spectral bands in new-generation hyperspectral sensors [1, 51, 56]. This reduction in spectral bandwidth results in each spectral channel capturing fewer photons, leading to higher levels of Poissonian noise. However, if the mean value of the photon counts is greater than four, Poissonian noise can be approximated as additive Gaussian noise with nearly constant variance by using variance-stabilizing transformations [43]. Therefore, in this paper, we assume that the observation

noise is additive Gaussian and sparse noise, then formulate the degradation model of HSI as follows:

$$\mathcal{Y} = \mathcal{X} + \mathcal{N} + \mathcal{S}, \quad (2)$$

where, $\mathcal{N} \in \mathbb{R}^{M \times N \times P}$ and $\mathcal{S} \in \mathbb{R}^{M \times N \times P}$ represent the imaging Gaussian noise and the sparse noise on the observation, respectively. Then the task of HSI denoising is given noisy HSI \mathcal{Y} to reconstruct the noisy free HSI \mathcal{X} .

3.2 Degradation-Noise-Aware Unfolding Network

Based on degradation (noise) model (2), we then formulate a principled Degradation Noise Aware Unfolding Network (DNA-Net) as depicted in Fig. 1. DNA-Net starts from the MAP theory. In particular, the original HSI signal could be estimated by minimizing the following energy function as follows:

$$\arg \min_{\mathcal{X}, \mathcal{N}, \mathcal{S}} \frac{1}{2} \|\mathcal{Y} - \mathcal{X} - \mathcal{N} - \mathcal{S}\|_{\text{F}}^2 + \tau \Phi(\mathcal{X}) + \lambda \|\mathcal{S}\|_1 + \gamma \|\mathcal{N}\|_{\text{F}}^2, \quad (3)$$

where $\frac{1}{2} \|\mathcal{Y} - \mathcal{X} - \mathcal{N} - \mathcal{S}\|_{\text{F}}^2$ is the data fidelity term, $\Phi(\mathcal{X})$ is the image prior term, $\|\mathcal{S}\|_1$, $\|\mathcal{N}\|_{\text{F}}^2$ are the modeling of Gaussian noise and Sparse noise, and τ, λ, γ are hyper-parameters balancing the importance. By introducing an auxiliary variable \mathcal{Z} , the sub-problem of \mathcal{X} in Eq. (3) can be reformulated as

$$\arg \min_{\mathcal{X}, \mathcal{Z}} \frac{1}{2} \|\mathcal{Y} - \mathcal{X} - \mathcal{N} - \mathcal{S}\|_{\text{F}}^2 + \tau \Phi(\mathcal{Z}), \text{ s.t. } \mathcal{Z} = \mathcal{X}. \quad (4)$$

This is a constrained optimization problem, it can be solved directly, but to obtain an unfolding inference, we adopt half-quadratic splitting (HQS) algorithm for its simplicity and fast convergence. Then Eq. (4) is solved by minimizing

$$\begin{aligned} \mathcal{L}_{\mu, \lambda, \beta}(\mathcal{X}, \mathcal{N}, \mathcal{S}) = & \frac{1}{2} \|\mathcal{Y} - \mathcal{X} - \mathcal{N} - \mathcal{S}\|_{\text{F}}^2 + \tau \Phi(\mathcal{Z}) + \lambda \|\mathcal{S}\|_1 \\ & + \gamma \|\mathcal{N}\|_{\text{F}}^2 + \frac{\mu}{2} \|\mathcal{Z} - \mathcal{X}\|^2, \end{aligned} \quad (5)$$

where μ is a penalty parameter that forces \mathcal{X} and \mathcal{Z} to approach the same fixed point. Subsequently, Eq. (5) can be solved by decoupling \mathcal{X} and \mathcal{Z} into the following two iterative sub-problems as

$$\begin{aligned} \mathcal{X}^{(k+1)} &= \arg \min_{\mathcal{X}} \|\mathcal{Y} - \mathcal{X} - \mathcal{N}^{(k)} - \mathcal{S}^{(k)}\|_{\text{F}}^2 + \mu \|\mathcal{X} - \mathcal{Z}^{(k)}\|^2, \\ \mathcal{Z}^{(k+1)} &= \arg \min_{\mathcal{Z}} \frac{\mu}{2} \|\mathcal{Z} - \mathcal{X}^{(k+1)}\|^2 + \tau \Phi(\mathcal{Z}), \end{aligned} \quad (6)$$

where $k = 0, 1, \dots, K-1$ indexes the iteration.

1) Update \mathcal{X} . For the data fidelity term, *i.e.*, \mathcal{X}_{k+1} in Eq. (6), it is associated with a quadratic regularized least-squares problem, which has a closed-form solution,

$$\mathcal{X}^{(k+1)} = \frac{\mathcal{Y} - \mathcal{N}^{(k)} - \mathcal{S}^{(k)} + \mu \mathcal{Z}^{(k)}}{1 + \mu}. \quad (7)$$

2) Update \mathcal{Z} . Extracting all terms containing \mathcal{Z} from the augmented Lagrangian function, one can get:

$$\mathcal{Z}^{(k+1)} = \arg \min_{\mathcal{Z}} \frac{\mu}{2\tau} \left\| \mathcal{Z} - \mathcal{X}^{(k+1)} \right\|_{\text{F}}^2 + \Phi(\mathcal{Z}). \quad (8)$$

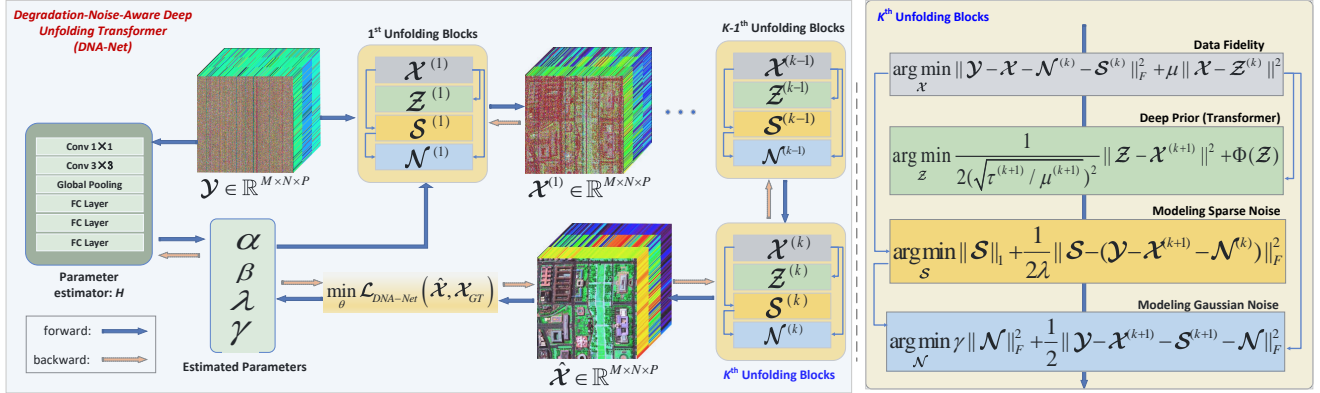


Figure 1: The architecture of our DNA-Net with K stages (iterations). H estimates informative parameters from the noisy HSI \mathcal{Y} and degradation matrix \mathbf{I} . The estimated parameters α , β , λ , and γ are fed into each stage of subsequent iterative learning.

We also set τ as iteration-specific parameters and \mathcal{Z}_{k+1} can be reformulated as

$$\mathcal{Z}^{(k+1)} = \arg \min_{\mathcal{Z}} \frac{1}{2(\sqrt{\tau^{(k+1)}}/\mu^{(k+1)})^2} \|\mathcal{Z} - \mathcal{X}^{(k+1)}\|^2 + \Phi(\mathcal{Z}). \quad (9)$$

From the perspective of Bayesian probability, Eq. (9) is equivalent to denoising image $\mathcal{X}^{(k+1)}$ with an Gaussian noise at level $\sqrt{\tau^{(k+1)}/\mu^{(k+1)}}$ [8]. Here, we customised an U-shaped transformer network (see Sec. 3.3 for details) to act as the denoiser, i.e.,

$$\mathcal{Z}^{(k+1)} = \mathcal{D}(\mathcal{X}^{(k+1)}, \sqrt{\tau^{(k+1)}/\mu^{(k+1)}}). \quad (10)$$

3) Update \mathcal{S} . By extracting all items related to \mathcal{S} from equation (5),

$$\mathcal{S}^{(k+1)} = \arg \min_{\mathcal{S}} \|\mathcal{S}\|_1 + \frac{1}{2\lambda} \|\mathcal{S} - (\mathcal{Y} - \mathcal{X}^{(k+1)} - \mathcal{N}^{(k)})\|_F^2. \quad (11)$$

By introducing the so-called soft-thresholding operator:

$$\mathcal{R}_{\Delta}(\mathbf{x}) = \begin{cases} x - \Delta, & \text{if } x > \Delta \\ x + \Delta, & \text{if } x < -\Delta \\ 0, & \text{otherwise} \end{cases} \quad (12)$$

where $x \in \mathbb{R}$ and $\Delta > 0$. Then we can update $\mathcal{S}^{(k+1)}$ as

$$\mathcal{S}^{(k+1)} = \mathcal{R}_{\lambda}(\mathcal{Y} - \mathcal{X}^{(k+1)} - \mathcal{N}^{(k)}). \quad (13)$$

4) Update \mathcal{N} , according to equation (5), we have

$$\mathcal{N}^{(k+1)} = \arg \min_{\mathcal{N}} \frac{1}{2} \|\mathcal{Y} - \mathcal{X} - \mathcal{N} - \mathcal{S}\|_F^2 + \gamma \|\mathcal{N}\|_F^2, \quad (14)$$

it has a closed-form solution,

$$\mathcal{N}^{(k+1)} = \frac{\mathcal{Y} - \mathcal{X}^{(k+1)} - \mathcal{S}^{(k+1)}}{1 + 2\gamma}. \quad (15)$$

Parameters estimation. The hyperparameters τ, λ, γ on Eq. (7), Eq. (10), Eq. (13), and Eq. (15), are used to weight the regularization terms to adjust the noise reduction strength on the noisy input, in order to minimize negative effects caused by noisy elements. However, the success of this weighting scheme is contingent upon prior knowledge and assumptions regarding the distribution of HSI noise. Consequently, these assumptions may not generalize well to diverse practical scenarios and can be biased towards complex real noises. To overcome this issue, we use a new data-driven approach for generalizing the weighting principle. We introduce an

explicit hyperweight estimation network that maps an input noisy image to appropriate weights for regularization, which consists of a $conv1 \times 1$, a strided $conv3 \times 3$, a global average pooling, and three fully connected layers, as shown in Fig. 1. This method seeks to capture the general weighting principle in a more objective manner. Specifically, based on Equation (6), the penalty parameter μ must satisfy a certain level of magnitude to ensure that the fixed points of \mathcal{X} and \mathcal{Z} converge closely. As such, μ serves as a crucial parameter that governs the convergence behavior and output quality of each iteration. To mitigate the need for manual tuning of μ , we automatically estimates μ based on a series of iteration-specific parameters derived from the HSI data. Specifically, we denote the value of μ in the k -th iteration as μ_k . Then, for estimating the parameters of Eq. (10), we set $\frac{1}{(\sqrt{\tau^{(k+1)}}/\mu^{(k+1)})^2} = \mu^{(k+1)}/\tau^{(k+1)}$ as parameters to be estimated from HSI. Let $\alpha^{(k)} \stackrel{\text{def}}{=} \mu^{(k)}$, $\boldsymbol{\alpha} \stackrel{\text{def}}{=} [\alpha^{(1)}, \dots, \alpha^{(k)}]$, $\beta^{(k)} \stackrel{\text{def}}{=} \mu^{(k)}/\tau^{(k)}$, and $\boldsymbol{\beta} \stackrel{\text{def}}{=} [\beta^{(1)}, \dots, \beta^{(k)}]$, $\boldsymbol{\gamma} \stackrel{\text{def}}{=} [\gamma^{(1)}, \dots, \gamma^{(k)}]$, $\boldsymbol{\lambda} \stackrel{\text{def}}{=} [\lambda^{(1)}, \dots, \lambda^{(k)}]$. Then we can formulate our DNA-Net as an iterative scheme:

$$\begin{aligned} (\boldsymbol{\alpha}, \boldsymbol{\beta}, \boldsymbol{\gamma}, \boldsymbol{\lambda}) &= \mathcal{H}(\mathcal{Y}, \mathbf{I}), \quad \mathcal{X}^{(k+1)} = \mathcal{F}(\mathcal{Y}, \mathcal{Z}^{(k)}, \boldsymbol{\alpha}^{(k+1)}, \mathbf{I}), \\ \mathcal{Z}^{(k+1)} &= \mathcal{D}(\mathcal{X}^{(k+1)}, \beta^{(k+1)}), \quad \mathcal{S}^{(k+1)} = \mathcal{R}(\mathcal{X}^{(k+1)}, \mathcal{N}^{(k)}, \lambda^{(k+1)}), \\ \mathcal{N}^{(k+1)} &= \mathcal{G}(\mathcal{X}^{(k+1)}, \mathcal{S}^{(k+1)}, \gamma^{(k+1)}), \end{aligned} \quad (16)$$

where \mathcal{H} denotes the parameter estimator that takes the noisy observation \mathcal{Y} and the identity degradation matrix \mathbf{I} of the HSI system as inputs, $\mathcal{F}, \mathcal{R}, \mathcal{G}$, equivalent to Eq. (7), Eq. (13), Eq. (15), and \mathcal{D} represents the Gaussian denoiser solving Eq. (10).

3.3 Customised HSI Transformer Denoiser

Previous approaches for designing denoiser priors for RGB image restoration have mainly utilized convolutional neural networks (CNNs), which have shown limited capacity to capture long-range dependencies [5] when it comes to HSI denoising task. While local and global Transformers can model long-range dependencies effectively, directly applying them to hyperspectral image (HSI) denoising faces two challenges: limited receptive fields and high computational costs. Moreover, the high spectral resolution of HSI suggests strong spectral correlation among spectral modes, which differs significantly from classic RGB images. Therefore, it is also

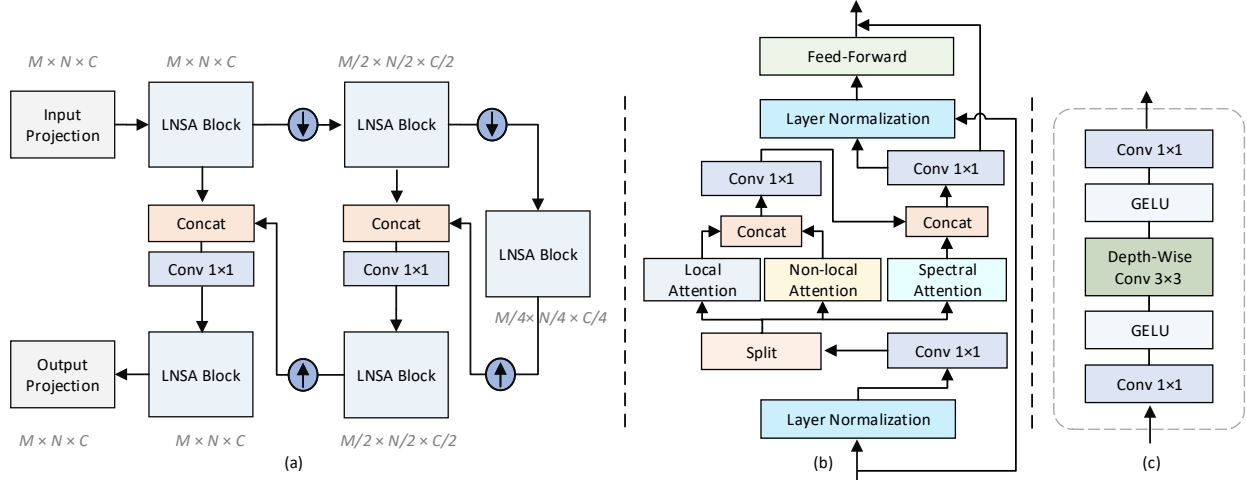


Figure 2: Diagram of the proposed transformer denoiser U-LSNA for our unfolding network DNA-Net. (a) U-LSNA adopts a U-shaped structure, (b) LNSA block, (c) Feed-forward network.

essential for the denoiser to model this critical feature of HSI. To address these challenges, we propose a novel U-shaped Local-Non-local-Spectral Transformer (U-LSNA) denoiser that utilizes a Local-Non-local-Spectral Attention (LNSA) mechanism. This approach combines local and non-local attention mechanisms with spectral convolution to capture long-range dependencies and strong spectral correlations while maintaining reasonable computational costs.

Overview of Denoiser U-LSNA. The architecture of U-LSNA is depicted in Fig.2 (a) and is built in a U-Net style by utilizing the proposed LNSA block as its fundamental unit. Given an input $\mathcal{X}^{(k+1)} \in \mathbb{R}^{M \times N \times C}$, U-LSNA first applies a $\text{conv}3 \times 3$ to map the concatenated reshaped $\mathcal{X}^{(k+1)}$ and stretched $\beta^{(k+1)}$ into feature $\mathcal{X}_0 \in \mathbb{R}^{M \times N \times C}$. Next, \mathcal{X}_0 is fed through the encoder, bottleneck, and decoder to be embedded into the deep feature $\mathcal{X}_d \in \mathbb{R}^{M \times N \times C}$. Each level of the encoder or decoder includes an LNSA and a resizing module. Fig.2 (b) shows that LNSA comprises of two layer normalization (LN) operations, an LNSA, and a Feed-Forward Network (FFN) that is explained in Fig. 2 (c). The downsampling and upsampling modules are implemented as strided $\text{conv}4 \times 4$ and $\text{deconv}2 \times 2$, respectively. Finally, a $\text{conv}3 \times 3$ is applied to \mathcal{X}_d to generate the residual image $\mathcal{T}^{(k+1)} \in \mathbb{R}^{M \times N \times C}$, and the output denoised image $\mathcal{Z}^{(k+1)}$ is obtained by adding reshaped $\mathcal{T}^{(k+1)}$ to $\mathcal{X}^{(k+1)}$: $\mathcal{Z}^{(k+1)} = \mathcal{T}^{(k+1)} + \mathcal{X}^{(k+1)}$.

Local-Nonlocal-Spectral-Attention. As the basic unit of U-LSNA, LNSA block is customised to model the local, non-local dependencies and spectral correlation of HSI by using a memory efficient group convolution mechanism. As depicted in Fig.2 (b), LNSA first feed input into a layer normalization (LN) block and a $\text{conv}1 \times 1$ layer, and then passes it into the parallel local-non-local attention layer and the spectral attention block, respectively. Subsequently, the outputs of local attention and non-local attention is concatenated and fused by a $\text{conv}1 \times 1$ layer, the fused outputs is concatenated with the output of spectral attention block and then fused by a $\text{conv}1 \times 1$ layer. Finally, a LN and a feed-forward layer are employed to generate the output of LNSA.

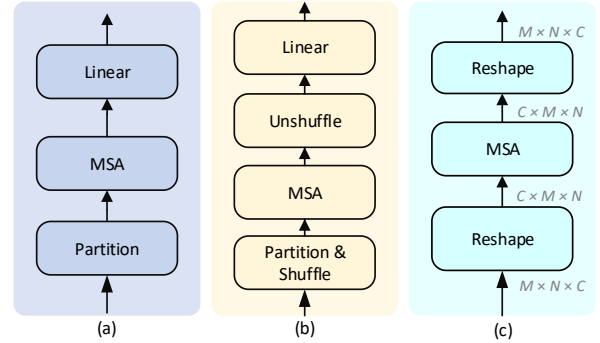


Figure 3: Diagram of (a) local attention structure. (b) non-local attention block. (c) spectral attention block, which are the key components of LNSA block.

Local-Non-local Attention Module. The input tokens of local-non-local-attention layer are denoted as $\mathcal{X}_{in} \in \mathbb{R}^{M \times N \times C}$. Subsequently, \mathcal{X}_{in} is linearly projected into *query* $Q \in \mathbb{R}^{M \times N \times C}$, *key* $\mathcal{K} \in \mathbb{R}^{M \times N \times C}$, and *value* $\mathcal{V} \in \mathbb{R}^{M \times N \times C}$ as

$$Q = \mathcal{X}_{in} \mathcal{W}^Q, \mathcal{K} = \mathcal{X}_{in} \mathcal{W}^{\mathcal{K}}, \mathcal{V} = \mathcal{X}_{in} \mathcal{W}^{\mathcal{V}}, \quad (17)$$

where $\mathcal{W}^Q, \mathcal{W}^{\mathcal{K}}, \mathcal{W}^{\mathcal{V}} \in \mathbb{R}^{C \times C}$ are learnable parameters and biases are omitted for simplification. Then, local contextual information and non-local dependencies are modeled by employing global MSA [24] and local window and shuffle-based MSA [4, 39]. The implementation of MSAs is parallelized to enhance efficiency. To this end, Q, \mathcal{K} , and \mathcal{V} are partitioned into two equal parts along the channel dimension,

$$Q = [Q_1, Q_2], \mathcal{K} = [\mathcal{K}_1, \mathcal{K}_2], \mathcal{V} = [\mathcal{V}_1, \mathcal{V}_2], \quad (18)$$

where $Q_1, \mathcal{K}_1, \mathcal{V}_1 \in \mathbb{R}^{M \times N \times \frac{C}{2}}$, $Q_2, \mathcal{K}_2, \mathcal{V}_2 \in \mathbb{R}^{M \times N \times \frac{C}{2}}$.

Then, $Q_1, \mathcal{K}_1, \mathcal{V}_1, Q_2, \mathcal{K}_2, \mathcal{V}_2$ are partitioned into non-overlapping windows of size $p \times p$, and reshaped into $\mathbb{R}^{\frac{MN}{p^2} \times p^2 \times \frac{C}{2}}$ firstly. However in non-local branch, $Q_2, \mathcal{K}_2, \mathcal{V}_2$ are transposed from $\mathbb{R}^{\frac{MN}{p^2} \times p^2 \times \frac{C}{2}}$

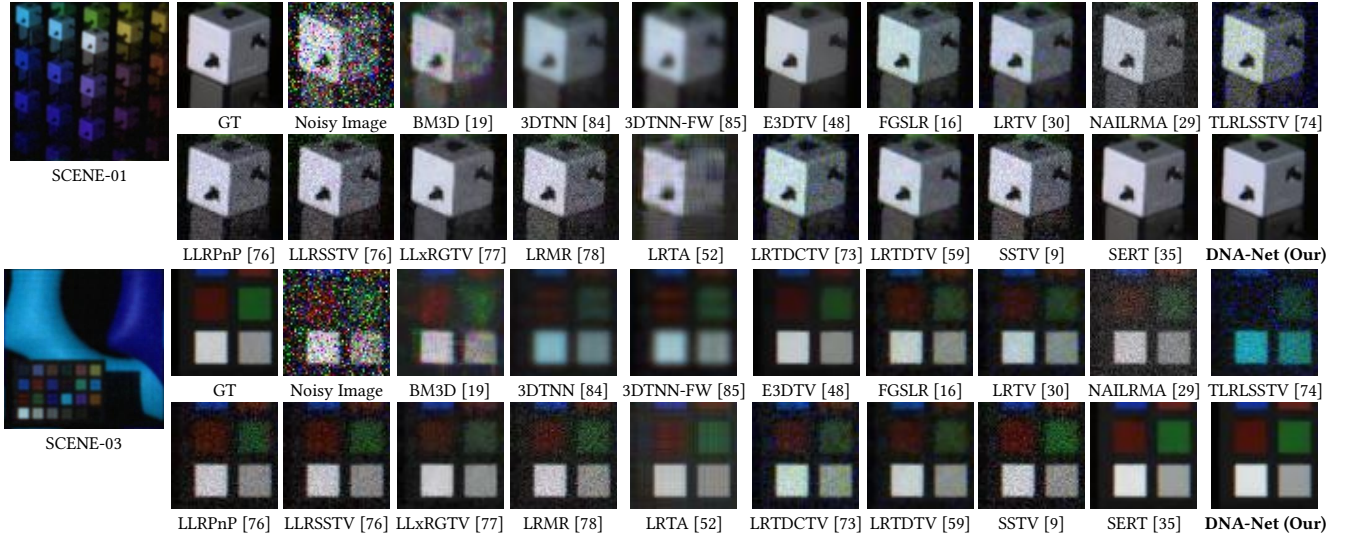


Figure 4: Visual comparison of HSI denoising methods.

to $\mathbb{R}^{p^2 \times \frac{MN}{p^2} \times \frac{C}{2}}$ to shuffle the positions of tokens and establish inter-window dependencies. Subsequently, $\mathcal{Q}_1, \mathcal{K}_1, \mathcal{V}_1$ and $\mathcal{Q}_2, \mathcal{K}_2, \mathcal{V}_2$ are split along the channel wise into h heads: $\mathcal{Q}_1 = [\mathcal{Q}_1^1, \dots, \mathcal{Q}_1^h]$, $\mathcal{K}_1 = [\mathcal{K}_1^1, \dots, \mathcal{K}_1^h]$, $\mathcal{V}_1 = [\mathcal{V}_1^1, \dots, \mathcal{V}_1^h]$. The dimension of each head is $d_h = \frac{C}{2h}$. $\mathcal{Q}_2, \mathcal{K}_2, \mathcal{V}_2$ are split into h heads: $\mathcal{Q}_2 = [\mathcal{Q}_2^1, \dots, \mathcal{Q}_2^h]$, $\mathcal{K}_2 = [\mathcal{K}_2^1, \dots, \mathcal{K}_2^h]$, $\mathcal{V}_2 = [\mathcal{V}_2^1, \dots, \mathcal{V}_2^h]$. The local and nonlocal self-attention \mathcal{A}_1^i and \mathcal{A}_2^i are calculated inside each head as

$$\begin{aligned} \mathcal{A}_1^i &= \text{softmax}\left(\frac{\mathcal{Q}_1^i \mathcal{K}_1^{i\top}}{\sqrt{d_h}} + \mathcal{P}_1^i\right) \mathcal{V}_1^i, \quad i = 1, \dots, h, \\ \mathcal{A}_2^i &= \text{softmax}\left(\frac{\mathcal{Q}_2^i \mathcal{K}_2^{i\top}}{\sqrt{d_h}} + \mathcal{P}_2^i\right) \mathcal{V}_2^i, \quad i = 1, \dots, h, \end{aligned} \quad (19)$$

where $\mathcal{P}_1^i \in \mathbb{R}^{p^2 \times p^2}$, $\mathcal{P}_2^i \in \mathbb{R}^{\frac{MN}{p^2} \times \frac{MN}{p^2}}$ are learnable parameters embedding the position information.

Spectral Prior Modeling Module. Meanwhile, a Global Spectral Self-Attention module (SM) is utilized in conjunction with the local-non-local branches to effectively capture the essential spectral correlations of HSI. Given an input $\mathcal{X}_{in} \in \mathbb{R}^{H \times W \times C}$, by using SM block, the input is firstly transposed and reshaped into $\mathcal{X}^T \in \mathbb{R}^{C \times HW}$. Subsequently, \mathcal{X}^T is linearly projected to $\mathcal{Q}^{sm} \in \mathbb{R}^{C \times HW}$, $\mathcal{K}^{sm} \in \mathbb{R}^{C \times HW}$, $\mathcal{V}^{sm} \in \mathbb{R}^{C \times HW}$ as: $\mathcal{Q}^{sm} = \mathcal{W}_q^{sm} \mathcal{X}^T$, $\mathcal{K}^{sm} = \mathcal{W}_k^{sm} \mathcal{X}^T$, $\mathcal{V}^{sm} = \mathcal{W}_v^{sm} \mathcal{X}^T$, where $\mathcal{W}_q, \mathcal{W}_k, \mathcal{W}_v \in \mathbb{R}^{C \times C}$. Then, $\mathcal{Q}^{sm}, \mathcal{K}^{sm}$, and \mathcal{V}^{sm} are split into N heads. The spectral attention of each head is computed as

$$\mathcal{A}_j^{sm} = \mathcal{V}_j^{sm} (\text{Softmax}(\mathcal{K}_j^{sm\top} \mathcal{Q}_j^{sm} / \sqrt{d})). \quad (20)$$

Subsequently, \mathcal{A}_j^{sm} are concatenated in spectral dimension and projected to generate the output \mathcal{X}_{sm} .

Finally, $\mathcal{A}_2^i \in \mathbb{R}^{p^2 \times \frac{MN}{p^2} \times d_h}$ is unshuffled by being transposed to shape $\mathbb{R}^{\frac{MN}{p^2} \times p^2 \times d_h}$, and the final result of LNSA is produced by aggregating the outputs of local-non-local attention in Eq. (19) and spectral prior modeling block,

$$\text{Conv } 1 \times 1 (\text{Concat}(\sum_{i=1}^h \mathcal{A}_1^i \mathcal{W}_1^i + \sum_{i=1}^h \mathcal{A}_2^i \mathcal{W}_2^i), \mathcal{X}_{sm}), \quad (21)$$

where $\mathcal{W}^i \in \mathbb{R}^{d_h \times C}$ are learnable parameters.

4 EXPERIMENT

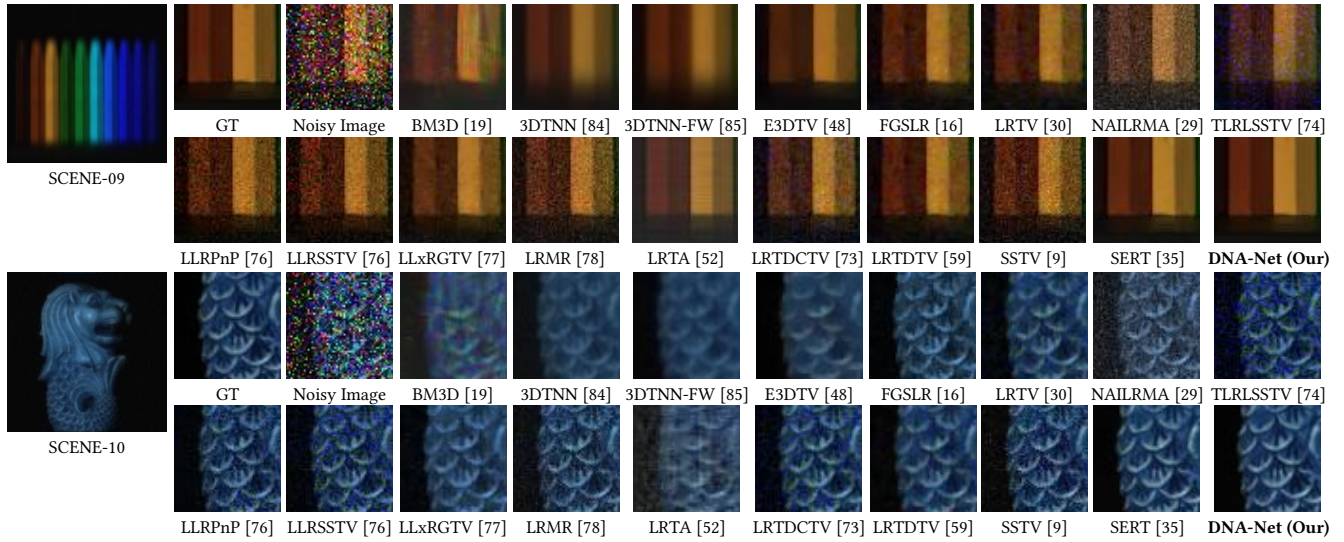
4.1 Experiment Setup

We employed HSI consisting of 28 wavelengths ranging from 450nm to 650nm, obtained through spectral interpolation. The performance of the proposed method was evaluated through both simulation and real experiments. Simulation experiments were conducted using two datasets, namely CAVE [47] and KAIST [17]. The CAVE dataset comprised 32 HSIs with spatial dimensions of 512×512, while the KAIST dataset contained 30 HSIs with spatial dimensions of 2704×3376. The CAVE dataset was utilized as the training set, whereas 10 scenes from the KAIST dataset were selected for testing purposes. Real experiments were conducted using Urban which had real noise. Pytorch was used to implement the proposed DNA-Net, which was trained with the Adam optimizer [32] and $\beta_1 = 0.9$ and $\beta_2 = 0.999$, for 110 epochs on a 2×GTX 1080Ti 11GB GPU using the Cosine Annealing scheme [40]. The training objective was to minimize the Root Mean Square Error (RMSE) between the denoised HSIs and the corresponding ground-truth HSIs.

4.2 Quantitative Comparisons with State-of-the-Art Methods

We compare the results of DNA-Net-B with 5 iterations, its light version DNA-Net-L with 2 iterations, and 18 SOTA methods including BM3D [19], LRTA [52], and LRTV [30], NAILRMA [29], LRMR [78], NonLRMA [15], LRTDTV [59], LLRSSTV [28], SSTV [9], TLR-LSSTV [74], and LLRPhP [76], LLxRGTV [77], 3DTNN [84], 3DTNN-FW [85], LRTDCTV [73], E3DTV [48], FGSLR [16], and SERT [35] on 10 simulation scenes and real noisy HSI-Urban.

Simulation HSI Denoising. *Noise cases.* Case-1: Gaussian noise $\mathcal{N}(0, 0.2)$, Case-2: Gaussian noise $\mathcal{N}(0, 0.2)$ + sparse (impulse) noise with $p = 0.05$, Case-3: Gaussian noise $\mathcal{N}(0, 0.2)$ + sparse noise with $p = 0.1$. Case-4: Gaussian noise $\mathcal{N}(0, 0.2)$ + sparse noise with $p = 0.15$. *Evaluation metrics.* We employed the widely-used quantitative


Figure 5: Visual comparison of HSI denoising methods.
Table 1: Comparisons under noise Case-1 and Case-2. PSNR, SSIM, FSIM, ERGAS and running time are reported.

(a) Comparisons on S10 under noise Case-1.

Method	PSNR \uparrow	SSIM \uparrow	FSIM \uparrow	ERGAS \downarrow	Time (s)
Noisy	16.094	0.110	0.426	807.880	-
BWBM3D [19]	23.037	0.348	0.825	367.630	0.527
LRTA [52]	21.302	0.267	0.691	438.080	3.205
LRTV [30]	28.351	0.535	0.810	205.025	9.442
NAILRMA [29]	23.215	0.407	0.822	356.335	8.632
LRMR [78]	24.416	0.387	0.785	307.134	59.763
NonLRMA [15]	27.897	0.725	0.883	204.716	16.043
LRTDTV [59]	30.147	0.618	0.861	159.869	43.858
LLRSSTV [28]	27.164	0.492	0.800	240.777	38.933
SSTV [9]	27.052	0.456	0.832	230.285	65.186
TLR-LSSTV [74]	27.981	0.539	0.821	218.898	100.600
LLRPnP [76]	28.735	0.608	0.897	193.391	0.530
LLxRGTV [77]	28.915	0.572	0.881	184.659	39.750
3DTNN [84]	25.326	0.436	0.848	278.152	17.160
3DTNN-FW [85]	27.754	0.538	0.850	209.240	22.227
LRTDCTV [73]	29.289	0.593	0.822	195.385	48.965
E3DTV [48]	28.996	0.854	0.878	189.818	9.288
FGSLR [16]	30.333	0.668	0.901	157.146	192.628
SERT [cvpr 2023][35]	41.448	0.969	0.986	44.423	0.306
DNA-Net-L (Ours)	41.614	0.986	0.989	43.452	0.082
DNA-Net-B (Ours)	42.332	0.988	0.990	40.445	0.205

(b) Comparisons on S3 under noise Case-2.

Method	PSNR \uparrow	SSIM \uparrow	FSIM \uparrow	ERGAS \downarrow	Time (s)
Noisy	13.515	0.056	0.292	982.660	0.000
BWBM3D [19]	23.754	0.609	0.889	318.304	0.509
LRTA [52]	22.581	0.564	0.864	363.086	0.431
LRTV [30]	28.978	0.588	0.769	162.753	10.316
NAILRMA [29]	21.765	0.359	0.710	384.629	9.010
LRMR [78]	24.616	0.396	0.716	257.022	63.121
NonLRMA [15]	20.626	0.429	0.774	447.370	17.475
LRTDTV [59]	31.199	0.682	0.828	119.344	47.167
LLRSSTV [28]	25.761	0.534	0.733	230.619	41.575
SSTV [9]	27.014	0.433	0.727	209.430	64.225
TLRLSSTV [74]	22.900	0.503	0.755	345.543	86.180
LLRPnP [76]	27.206	0.634	0.807	189.142	0.583
LLxRGTV [77]	30.657	0.732	0.886	128.963	46.797
3DTNN [84]	26.138	0.703	0.898	225.699	22.766
3DTNN-FW [85]	29.123	0.810	0.895	151.480	25.897
LRTDCTV [73]	27.382	0.474	0.697	192.751	65.079
E3DTV [48]	32.634	0.907	0.942	168.679	11.667
FGSLR [16]	31.617	0.727	0.860	115.760	285.600
SERT [cvpr 2023][35]	43.126	0.971	0.978	35.227	0.302
DNA-Net-L (Ours)	43.888	0.980	0.979	31.632	0.091
DNA-Net-B (Ours)	44.658	0.981	0.979	30.165	0.214

picture quality indices (PQIs): PSNR, SSIM, FSIM [81], ERGAS [58] metrics to evaluate the denoising performance quantitatively.

Tables 1 and 3 depict the outcomes of experiments on scenes 1 to 10 of the KAIST dataset, aimed at removing mixed Gaussian and sparse noise. Our proposed DNA-Net model was compared against several SOTA denoising approaches. The DNA-Net-B model attained PSNR values of 42.33 dB, 44.66 dB, 44.17 dB, and 43.78 dB, surpassing all other methods by an average of 1.49 dB. Moreover, with respect to SSIM, DNA-Net outperformed the recently proposed state-of-the-art SERT method [35] by a minimum of 0.1.

Visual analysis of the results is presented in Fig. 4 and 5, which demonstrate the efficacy of DNA-Net in reducing mixed noise while preserving the details of HSI. To evaluate whether the enhanced performance was obtained at the expense of increased computational

costs, we compared the PQIs results against computational cost, which are shown in Tables 1 and 3. The DNA-Net-L model delivered superior performance compared to most models, with the lowest computational cost, highlighting its efficiency and effectiveness.

Real HSI Denoising. The HYDICE Urban hyperspectral imagery dataset ¹ has an original size of $207 \times 207 \times 210$, with 189 bands remaining after excluding the water absorption band. Fig. 6 displays grayscale images of the 108th band in the noisy HSI and the results after applying various restoration methods. Among these methods, the DNA-Net method is particularly effective in removing sparse noise, especially strip noise, and restoring spatial details, resulting in the best visual quality of the restored image.

¹<http://www.tec.army.mil/hypercube/>

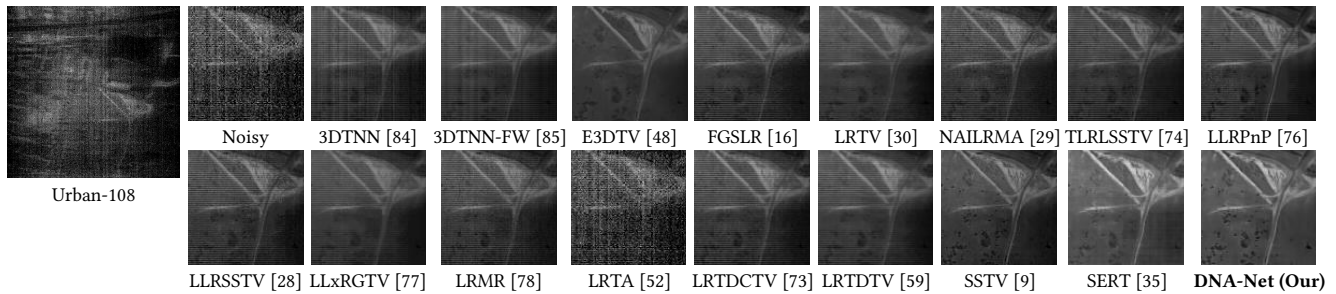


Figure 6: Visual comparison of HSI denoising methods on real noisy HSI Urban.

Table 2: Ablation studies on Scene 10 of simulation datasets [17]. PSNR, SSIM, FSIM, ERGAS are reported.

DNA-Net	Local Attention	Non-local Attention	Spectral Attention	PSNR \uparrow	SSIM \uparrow	FSIM \uparrow	ERGAS \downarrow
\checkmark	\checkmark			40.300	0.972	0.981	50.089
\checkmark	\checkmark		\checkmark	41.247	0.978	0.986	45.116
\checkmark	\checkmark	\checkmark		40.563	0.973	0.985	49.236
\checkmark	\checkmark	\checkmark	\checkmark	41.489	0.986	0.988	44.106

Table 3: Comparisons under noise Case-3 and Case-4. PSNR, SSIM, FSIM, ERGAS and running time are reported.

(a) Comparisons on S1 under noise Case-3.

(b) Comparisons on S9 under noise Case-4.

Method	PSNR \uparrow	SSIM \uparrow	FSIM \uparrow	ERGAS \downarrow	Time (s)
Noisy	11.830	0.045	0.331	1324.192	-
BWBM3D [19]	21.309	0.449	0.790	445.832	0.611
LRTA [52]	20.310	0.481	0.827	499.671	0.479
LRTV [30]	28.872	0.617	0.806	225.460	9.302
NAILRMA [29]	20.055	0.318	0.708	513.617	10.896
LRMR [78]	24.204	0.400	0.745	317.549	60.537
NonLRMA [15]	22.746	0.388	0.773	376.698	9.768
LRTDTV [59]	30.629	0.695	0.848	154.044	43.426
LLRSSTV [28]	26.010	0.510	0.754	288.215	40.266
SSTV [9]	26.669	0.474	0.781	239.868	63.276
TLR-LSSTV [74]	25.284	0.461	0.732	407.490	85.206
LLRPhP [76]	27.275	0.643	0.832	243.813	0.748
LLxRGTV[77]	29.296	0.705	0.890	176.948	45.746
3DTNN[84]	26.739	0.671	0.863	237.061	20.755
3DTNN-FW[85]	29.730	0.775	0.869	168.599	25.228
LRTDCTV [73]	28.187	0.562	0.785	231.739	59.314
E3DTV [48]	30.820	0.852	0.876	151.999	10.955
FGSLR [16]	30.909	0.729	0.872	146.890	379.678
SERT [cvpr 2023][35]	42.350	0.969	0.984	45.665	0.293
DNA-Net-L (Ours)	43.072	0.981	0.988	42.095	0.086
DNA-Net-B (Ours)	44.168	0.983	0.989	37.242	0.212

Method	PSNR \uparrow	SSIM \uparrow	FSIM \uparrow	ERGAS \downarrow	Time (s)
Noisy	10.688	0.034	0.247	1493.682	-
BWBM3D [19]	19.239	0.281	0.677	558.502	0.563
LRTA [52]	18.721	0.465	0.882	595.824	0.272
LRTV [30]	27.957	0.535	0.729	217.996	9.498
NAILRMA [29]	17.972	0.233	0.613	646.518	11.025
LRMR [78]	22.666	0.355	0.669	372.022	60.654
NonLRMA [15]	21.950	0.453	0.747	453.460	13.077
LRTDTV [59]	30.086	0.637	0.788	161.100	47.716
LLRSSTV [28]	23.405	0.546	0.700	361.783	40.168
SSTV [9]	26.341	0.406	0.707	244.761	64.891
TLR-LSSTV [74]	26.008	0.585	0.763	286.956	87.575
LLRPhP [76]	25.414	0.674	0.791	287.431	0.599
LLxRGTV [77]	29.750	0.682	0.875	163.572	48.340
3DTNN [84]	26.068	0.643	0.897	251.031	22.845
3DTNN-FW [85]	28.953	0.759	0.882	179.162	28.159
LRTDCTV [73]	25.592	0.398	0.644	279.517	67.074
E3DTV [48]	30.343	0.879	0.915	189.866	11.735
FGSLR [16]	29.914	0.632	0.804	160.725	491.061
SERT [cvpr 2023][35]	41.987	0.969	0.977	42.999	0.318
DNA-Net-L (Ours)	41.952	0.980	0.981	43.734	0.086
DNA-Net-B (Ours)	43.780	0.983	0.984	35.252	0.210

5 ABLATION STUDY

Component Ablation. Table 2 presents the results of various component designs. The first row corresponds to the proposed DNA-Net that solely utilizes local attention in the spatial domain. The 2nd, 3rd, and 4th rows represent DNA-Net models that incorporate additional spectral attention, non-local attention, and spectral plus non-local attention, respectively. The results demonstrate that incorporating spectral and non-local attention blocks to capture spatial-spectral information significantly improves the denoising performance.

Iteration Analysis. In Tables 1 and 3, the performance of DNA-Net with 2 and 5 iterations, denoted as DNA-Net-L and DNA-Net-B, respectively, is presented in the last two rows. The results indicate that DNA-Net-B displays an enhancement in PQIs, albeit at the

expense of increased running time. Therefore, selecting the appropriate iteration model for a given application in practical scenarios requires a trade-off between speed and performance.

6 CONCLUSION

This paper addresses three issues that arise in previous model-based or learning-based HSI denoising methods. These issues include a lack of informative parameter estimation for iterative learning, the inability to model noise distributions, and limitations in capturing long-range dependencies due to their primary reliance on CNN-based approaches. To overcome these challenges, we propose a new MAP-based unfolding framework called DNA-Net. The DNA-Net framework is capable of effectively modeling both sparse and Gaussian noise distributions and accurately estimating parameters

from a noisy HSI and degradation matrix. These estimated parameters are subsequently utilized to contextualize the effect of noise terms and provide important noise level information for the denoising network during each iteration. Furthermore, we introduce a new Transformer-based method, U-LNSA, which is capable of jointly extracting spectral correlation, presenting local contents, and modeling non-local dependencies. By integrating U-LNSA into the DNA-Net framework, we present the first Transformer-based unfolding method for HSI denoising. Experimental results clearly indicate that the proposed DNA-Net approach outperforms state-of-the-art methods by a significant margin while requiring much lower memory and computational costs.

REFERENCES

- [1] Nicola Acito, Marco Diani, and Giovanni Corsini. 2011. Signal-dependent noise modeling and model parameter estimation in hyperspectral images. *IEEE Transactions on Geoscience and Remote Sensing* 49, 8 (2011), 2957–2971.
- [2] Anurag Arnab, Mostafa Dehghani, Georg Heigold, Chen Sun, Mario Lučić, and Cordelia Schmid. 2021. Vivit: A video vision transformer. *arXiv preprint arXiv:2103.15691* (2021).
- [3] Théo Bodrito, Alexandre Zouaoui, Jocelyn Chanusot, and Julien Mairal. 2021. A trainable spectral-spatial sparse coding model for hyperspectral image restoration. *Advances in Neural Information Processing Systems* 34 (2021), 5430–5442.
- [4] Yuanhao Cai, Jing Lin, Xiaowan Hu, Haoqian Wang, Xin Yuan, Yulun Zhang, Radu Timofte, and Luc Van Gool. 2022. Mask-guided Spectral-wise Transformer for Efficient Hyperspectral Image Reconstruction. In *CVPR*.
- [5] Yuanhao Cai, Jing Lin, Haoqian Wang, Xin Yuan, Henghui Ding, Yulun Zhang, Radu Timofte, and Luc V Gool. 2022. Degradation-aware unfolding half-shuffle transformer for spectral compressive imaging. *Advances in Neural Information Processing Systems* 35 (2022), 37749–37761.
- [6] Hu Cao, Yueyue Wang, Joy Chen, Dongsheng Jiang, Xiaopeng Zhang, Qi Tian, and Manning Wang. 2021. Swin-Unet: Unet-like Pure Transformer for Medical Image Segmentation. *arXiv preprint arXiv:2105.05537* (2021).
- [7] Stanley H Chan, Xiran Wang, and Omar A Elgandy. 2016. Plug-and-play ADMM for image restoration: Fixed-point convergence and applications. *IEEE Transactions on Computational Imaging* 3, 1 (2016), 84–98.
- [8] Stanley H Chan, Xiran Wang, and Omar A Elgandy. 2016. Plug-and-play ADMM for image restoration: Fixed-point convergence and applications. *Transactions on Computational Imaging* (2016).
- [9] Yi Chang, Luxin Yan, Houzhang Fang, and Chunan Luo. 2015. Anisotropic spectral-spatial total variation model for multispectral remote sensing image destriping. *IEEE Transactions on Image Processing* 24, 6 (2015), 1852–1866.
- [10] Yi Chang, Luxin Yan, Houzhang Fang, Sheng Zhong, and Wenshan Liao. 2018. HSI-DeNet: Hyperspectral image restoration via convolutional neural network. *IEEE Transactions on Geoscience and Remote Sensing* 57, 2 (2018), 667–682.
- [11] Yi Chang, Luxin Yan, Xi-Le Zhao, Houzhang Fang, Zhijun Zhang, and Sheng Zhong. 2020. Weighted low-rank tensor recovery for hyperspectral image restoration. *IEEE Transactions on Cybernetics* 50, 11 (2020), 4558–4572.
- [12] Hanting Chen, Yunhe Wang, Tianyu Guo, Chang Xu, Yiping Deng, Zhenhua Liu, Siwei Ma, Chunjing Xu, Chao Xu, and Wen Gao. 2021. Pre-Trained Image Processing Transformer. In *CVPR*.
- [13] Hongyu Chen, Guangyi Yang, and Hongyan Zhang. 2022. Hider: A hyperspectral image denoising transformer with spatial-spectral constraints for hybrid noise removal. *IEEE Transactions on Neural Networks and Learning Systems* (2022).
- [14] Yang Chen, Xiangyong Cao, Qian Zhao, Deyu Meng, and Zongben Xu. 2017. Denoising hyperspectral image with non-iid noise structure. *IEEE Transactions on Cybernetics* 48, 3 (2017), 1054–1066.
- [15] Yongyong Chen, Yanwen Guo, Yongli Wang, Dong Wang, Chong Peng, and Guoping He. 2017. Denoising of hyperspectral images using nonconvex low rank matrix approximation. *IEEE Transactions on Geoscience and Remote Sensing* 55, 9 (2017), 5366–5380.
- [16] Yong Chen, Ting-Zhu Huang, Wei He, Xi-Le Zhao, Hongyan Zhang, and Jinshan Zeng. 2021. Hyperspectral image denoising using factor group sparsity-regularized nonconvex low-rank approximation. *IEEE Transactions on Geoscience and Remote Sensing* 60 (2021), 1–16.
- [17] Inchang Choi, MH Kim, D Gutierrez, DS Jeon, and G Nam. 2017. High-quality hyperspectral reconstruction using a spectral prior. In *Technical report*.
- [18] Daniel Coquelin, Behnood Rasti, Markus Götz, Pedram Ghamisi, Richard Gloaguen, and Achim Streit. 2022. HyDe: The first open-source, Python-based, GPU-accelerated hyperspectral denoising package. In *2022 12th Workshop on Hyperspectral Imaging and Signal Processing: Evolution in Remote Sensing (WHISPERS)*. IEEE, 1–5.
- [19] Kostadin Dabov, Alessandro Foi, Vladimir Katkovnik, and Karen Egiazarian. 2007. Image denoising by sparse 3-D transform-domain collaborative filtering. *IEEE Transactions on image processing* 16, 8 (2007), 2080–2095.
- [20] Kostadin Dabov, Alessandro Foi, Vladimir Katkovnik, and Karen Egiazarian. 2007. Image denoising by sparse 3-D transform-domain collaborative filtering. *IEEE Transactions on Image Processing* 16, 8 (2007), 2080–2095.
- [21] Aram Danielyan, Vladimir Katkovnik, and Karen Egiazarian. 2010. Image deblurring by augmented Lagrangian with BM3D frame prior. In *Proceedings of the Workshop on Information Theoretic Methods in Science and Engineering*, Vol. 1.
- [22] Zhuo Deng, Yuanhao Cai, Lu Chen, Zheng Gong, Qiqi Bao, Xue Yao, Dong Fang, Shaochong Zhang, and Lan Ma. 2022. RFormer: Transformer-based Generative Adversarial Network for Real Fundus Image Restoration on A New Clinical Benchmark. *arXiv preprint arXiv:2201.00466* (2022).
- [23] Weisheng Dong, Huan Wang, Fangfang Wu, Guangming Shi, and Xin Li. 2019. Deep spatial-spectral representation learning for hyperspectral image denoising. *IEEE Transactions on Computational Imaging* 5, 4 (2019), 635–648.
- [24] Alexey Dosovitskiy, Lucas Beyer, Alexander Kolesnikov, Dirk Weissenborn, Xi-aohua Zhai, Thomas Unterthiner, Mostafa Dehghani, Matthias Minderer, Georg Heigold, Sylvain Gelly, Jakob Uszkoreit, and Neil Houlsby. 2021. An Image is Worth 16x16 Words: Transformers for Image Recognition at Scale. In *ICLR*.
- [25] Guanyiman Fu, Fengchao Xiong, Jianfeng Lu, Jun Zhou, and Yuntao Qian. 2022. Nonlocal spatial-spectral neural network for hyperspectral image denoising. *IEEE Transactions on Geoscience and Remote Sensing* 60 (2022), 1–16.
- [26] Ying Fu, Antony Lam, Imari Sato, and Yoichi Sato. 2017. Adaptive spatial-spectral dictionary learning for hyperspectral image restoration. *International Journal of Computer Vision* 122, 2 (2017), 228–245.
- [27] Wei He, Quanming Yao, Chao Li, Naoto Yokoya, and Qibin Zhao. 2019. Non-local meets global: An integrated paradigm for hyperspectral denoising. In *Proceedings of the IEEE Conference on Computer Vision and Pattern Recognition*. 6868–6877.
- [28] Wei He, Hongyan Zhang, Huanfeng Shen, and Liangpei Zhang. 2018. Hyperspectral image denoising using local low-rank matrix recovery and global spatial-spectral total variation. *IEEE Journal of Selected Topics in Applied Earth Observations and Remote Sensing* 11, 3 (2018), 713–729.
- [29] Wei He, Hongyan Zhang, Liangpei Zhang, and Huanfeng Shen. 2015. Hyperspectral image denoising via noise-adjusted iterative low-rank matrix approximation. *IEEE Journal of Selected Topics in Applied Earth Observations and Remote Sensing* 8, 6 (2015), 3050–3061.
- [30] Wei He, Hongyan Zhang, Liangpei Zhang, and Huanfeng Shen. 2015. Total-variation-regularized low-rank matrix factorization for hyperspectral image restoration. *IEEE transactions on geoscience and remote sensing* 54, 1 (2015), 178–188.
- [31] Wei He, Hongyan Zhang, Liangpei Zhang, and Huanfeng Shen. 2015. Total-variation-regularized low-rank matrix factorization for hyperspectral image restoration. *IEEE Transactions on Geoscience and Remote Sensing* 54, 1 (2015), 178–188.
- [32] Diederik P. Kingma and Jimmy Lei Ba. 2015. Adam: A Method for Stochastic Optimization. In *ICLR*.
- [33] Zeqiang Lai and Ying Fu. 2023. Mixed Attention Network for Hyperspectral Image Denoising. *arXiv preprint arXiv:2301.11525* (2023).
- [34] Zeqiang Lai, Kaixuan Wei, and Ying Fu. 2022. Deep plug-and-play prior for hyperspectral image restoration. *Neurocomputing* 481 (2022), 281–293.
- [35] Miaoyu Li, Ji Liu, Ying Fu, Yulun Zhang, and Dejing Dou. 2023. Spectral Enhanced Rectangle Transformer for Hyperspectral Image Denoising. *arXiv preprint arXiv:2304.00844* (2023).
- [36] Yanjie Li, Shoukui Zhang, Zhicheng Wang, Sen Yang, Wankou Yang, Shu-Tao Xia, and Erjin Zhou. 2021. TokenPose: Learning Keypoint Tokens for Human Pose Estimation. In *ICCV*.
- [37] Liang Liang, Liping Di, Lianpeng Zhang, Meixia Deng, Zhihao Qin, Shuhe Zhao, and Hui Lin. 2015. Estimation of crop LAI using hyperspectral vegetation indices and a hybrid inversion method. *Remote Sensing of Environment* 165 (2015), 123–134.
- [38] YunYang Liu, XiLe Zhao, YuBang Zheng, TianHui Ma, and Hongyan Zhang. 2021. Hyperspectral Image Restoration by Tensor Fibered Rank Constrained Optimization and Plug-and-Play Regularization. *IEEE Transactions on Geoscience and Remote Sensing* (2021), 1–17.
- [39] Ze Liu, Yutong Lin, Yue Cao, Han Hu, Yixuan Wei, Zheng Zhang, Stephen Lin, and Baining Guo. 2021. Swin transformer: Hierarchical vision transformer using shifted windows. In *Proceedings of the IEEE/CVF International Conference on Computer Vision*. 10012–10022.
- [40] Ilya Loshchilov and Frank Hutter. 2017. Sgdr: Stochastic gradient descent with warm restarts. In *ICLR*.
- [41] TianHui Ma, Zongben Xu, Deyu Meng, and XiLe Zhao. 2020. Hyperspectral Image Restoration Combining Intrinsic Image Characterization With Robust Noise Modeling. *IEEE Journal of Selected Topics in Applied Earth Observations and Remote Sensing* 14 (2020), 1628–1644.
- [42] Matteo Maggioni, Vladimir Katkovnik, Karen Egiazarian, and Alessandro Foi. 2012. Nonlocal transform-domain filter for volumetric data denoising and reconstruction. *IEEE Transactions on Image Processing* 22, 1 (2012), 119–133.

- [43] Markku Makitalo and Alessandro Foi. 2011. A closed-form approximation of the exact unbiased inverse of the Anscombe variance-stabilizing transformation. *IEEE transactions on image processing* 20, 9 (2011), 2697–2698.
- [44] Hisham Othman and Shen-En Qian. 2006. Noise reduction of hyperspectral imagery using hybrid spatial-spectral derivative-domain wavelet shrinkage. *IEEE Transactions on Geoscience and Remote Sensing* 44, 2 (2006), 397–408.
- [45] Erting Pan, Yong Ma, Xiaoguang Mei, Fan Fan, Jun Huang, and Jiayi Ma. 2022. SQAD: Spatial-Spectral Quasi-Attention Recurrent Network for Hyperspectral Image Denoising. *IEEE Transactions on Geoscience and Remote Sensing* 60 (2022), 1–14. <https://doi.org/10.1109/TGRS.2022.3156646>
- [46] Li Pang, Weizhen Gu, and Xiangyong Cao. 2022. TRQ3DNet: A 3D Quasi-Recurrent and Transformer Based Network for Hyperspectral Image Denoising. *IEEE Transactions on Geoscience and Remote Sensing* 60 (2022), 4598.
- [47] Jong-Il Park, Moon-Hyun Lee, Michael D. Grossberg, and Shree K. Nayar. 2007. Multispectral Imaging Using Multiplexed Illumination. In *ICCV*.
- [48] Jiangjun Peng, Qi Xie, Qian Zhao, Yao Wang, Leung Yee, and Deyu Meng. 2020. Enhanced 3DTV regularization and its applications on HSI denoising and compressed sensing. *IEEE Transactions on Image Processing* 29 (2020), 7889–7903.
- [49] J. Peng, Q. Xie, Q. Zhao, Y. Wang, L. Yee, and D. Meng. 2020. Enhanced 3DTV Regularization and Its Applications on HSI Denoising and Compressed Sensing. *IEEE Transactions on Image Processing* 29 (2020), 7889–7903.
- [50] Yi Peng, Deyu Meng, Zongben Xu, Chenqiang Gao, Yi Yang, and Biao Zhang. 2014. Decomposable nonlocal tensor dictionary learning for multispectral image denoising. In *Proceedings of the IEEE Conference on Computer Vision and Pattern Recognition*. 2949–2956.
- [51] Yuntao Qian and Minchao Ye. 2012. Hyperspectral imagery restoration using nonlocal spectral-spatial structured sparse representation with noise estimation. *IEEE Journal of Selected Topics in Applied Earth Observations and Remote Sensing* 6, 2 (2012), 499–515.
- [52] Nadine Renard, Salah Bourennane, and Jacques Blanc-Talon. 2008. Denoising and dimensionality reduction using multilinear tools for hyperspectral images. *IEEE Geoscience and Remote Sensing Letters* 5, 2 (2008), 138–142.
- [53] Xiangyu Rui, Xiangyong Cao, Jun Shu, Qian Zhao, and Deyu Meng. 2022. A Hyper-weight Network for Hyperspectral Image Denoising. *arXiv preprint arXiv:2301.06081* (2022).
- [54] Le Sun, Byeungwoo Jeon, Yuhui Zheng, and Zebin Wu. 2017. Hyperspectral image restoration using low-rank representation on spectral difference image. *IEEE Geoscience and Remote Sensing Letters* 14, 7 (2017), 1151–1155.
- [55] Ying Tai, Jian Yang, Xiaoming Liu, and Chunyan Xu. 2017. Memnet: A persistent memory network for image restoration. In *Proceedings of the IEEE international conference on computer vision*. 4539–4547.
- [56] Mikhail L. Uss, Benoît Vozel, Vladimir V. Lukin, and Kacem Chehdi. 2011. Local signal-dependent noise variance estimation from hyperspectral textural images. *IEEE Journal of Selected Topics in Signal Processing* 5, 3 (2011), 469–486.
- [57] Ashish Vaswani, Noam Shazeer, Niki Parmar, Jakob Uszkoreit, Llion Jones, Aidan N Gomez, Lukasz Kaiser, and Illia Polosukhin. 2017. Attention is all you need. *Advances in neural information processing systems* 30 (2017).
- [58] Lucien Wald. 2002. *Data fusion: definitions and architectures: fusion of images of different spatial resolutions*. Presses des MINES.
- [59] Yao Wang, Jiangjun Peng, Qian Zhao, Yee Leung, Xi-Le Zhao, and Deyu Meng. 2017. Hyperspectral image restoration via total variation regularized low-rank tensor decomposition. *IEEE Journal of Selected Topics in Applied Earth Observations and Remote Sensing* 11, 4 (2017), 1227–1243.
- [60] Zhendong Wang, Xiaodong Cun, Jianmin Bao, Wengang Zhou, Jianzhuang Liu, and Houqiang Li. 2022. Uformer: A general u-shaped transformer for image restoration. In *Proceedings of the IEEE/CVF Conference on Computer Vision and Pattern Recognition*. 17683–17693.
- [61] Kaixuan Wei and Ying Fu. 2019. Low-rank Bayesian tensor factorization for hyperspectral image denoising. *Neurocomputing* 331 (2019), 412–423.
- [62] Kaixuan Wei, Ying Fu, and Hua Huang. 2021. 3-D Quasi-Recurrent Neural Network for Hyperspectral Image Denoising. *IEEE Transactions on Neural Networks and Learning Systems* 32, 1 (2021), 363–375.
- [63] Enze Xie, Wenhai Wang, Zhiding Yu, Anima Anandkumar, Jose M Alvarez, and Ping Luo. 2021. SegFormer: Simple and efficient design for semantic segmentation with transformers. In *NeurIPS*.
- [64] Fengchao Xiong, Jun Zhou, Shuyin Tao, Jianfeng Lu, Jiantao Zhou, and Yuntao Qian. 2022. SMDs-Net: Model guided spectral-spatial network for hyperspectral image denoising. *IEEE Transactions on Image Processing* 31 (2022), 5469–5483.
- [65] Fengchao Xiong, Jun Zhou, Shuyin Tao, Jianfeng Lu, Jiantao Zhou, and Yuntao Qian. 2022. SMDs-Net: Model guided spectral-spatial network for hyperspectral image denoising. *IEEE Transactions on Image Processing* 31 (2022), 5469–5483.
- [66] Fengchao Xiong, Jun Zhou, Qinling Zhao, Jianfeng Lu, and Yuntao Qian. 2021. MAC-Net: Model-aided nonlocal neural network for hyperspectral image denoising. *IEEE Transactions on Geoscience and Remote Sensing* 60 (2021), 1–14.
- [67] Sen Yang, Zhibin Quan, Mu Nie, and Wankou Yang. 2021. TransPose: Keypoint Localization via Transformer. In *ICCV*.
- [68] Xiguang Yang and Ying Yu. 2017. Estimating soil salinity under various moisture conditions: An experimental study. *IEEE Transactions on Geoscience and Remote Sensing* 55, 5 (2017), 2525–2533.
- [69] Zongxin Yang, Yunchao Wei, and Yi Yang. 2021. Associating objects with transformers for video object segmentation. In *NeurIPS*.
- [70] Naoto Yokoya, Jonathan Cheung-Wai Chan, and Karl Segl. 2016. Potential of resolution-enhanced hyperspectral data for mineral mapping using simulated EnMAP and Sentinel-2 images. *Remote Sensing* 8, 3 (2016), 172.
- [71] Qiangqiang Yuan, Liangpei Zhang, and Huanfeng Shen. 2012. Hyperspectral image denoising employing a spectral-spatial adaptive total variation model. *IEEE Transactions on Geoscience and Remote Sensing* 50, 10 (2012), 3660–3677.
- [72] Qiangqiang Yuan, Qiang Zhang, Jie Li, Huanfeng Shen, and Liangpei Zhang. 2018. Hyperspectral image denoising employing a spatial-spectral deep residual convolutional neural network. *IEEE Transactions on Geoscience and Remote Sensing* 57, 2 (2018), 1205–1218.
- [73] Haijin Zeng, Shaoguang Huang, Yongyong Chen, Hiep Luong, and Wilfried Philips. 2022. Low-rank Meets Sparseness: An Integrated Spatial-Spectral Total Variation Approach to Hyperspectral Denoising. *arXiv preprint arXiv:2204.12879* (2022).
- [74] Haijin Zeng, Xiaozhen Xie, Haojie Cui, Hanping Yin, and Jifeng Ning. 2020. Hyperspectral image restoration via global L 1-2 spatial-spectral total variation regularized local low-rank tensor recovery. *IEEE Transactions on Geoscience and Remote Sensing* 59, 4 (2020), 3309–3325.
- [75] Haijin Zeng, Xiaozhen Xie, Haojie Cui, Yuan Zhao, and Jifeng Ning. 2020. Hyperspectral image restoration via CNN denoiser prior regularized low-rank tensor recovery. *Computer Vision and Image Understanding* 197 (2020), 103004.
- [76] Haijin Zeng, Xiaozhen Xie, Wenfeng Kong, Shuang Cui, and Jifeng Ning. 2020. Hyperspectral image denoising via combined non-local self-similarity and local low-rank regularization. *IEEE Access* 8 (2020), 50190–50208.
- [77] Haijin Zeng, Xiaozhen Xie, and Jifeng Ning. 2021. Hyperspectral image denoising via global spatial-spectral total variation regularized nonconvex local low-rank tensor approximation. *Signal Processing* 178 (2021), 107805.
- [78] Hongyan Zhang, Wei He, Liangpei Zhang, Huanfeng Shen, and Qiangqiang Yuan. 2013. Hyperspectral image restoration using low-rank matrix recovery. *IEEE transactions on geoscience and remote sensing* 52, 8 (2013), 4729–4743.
- [79] Kai Zhang, Wangmeng Zuo, Yunjin Chen, Deyu Meng, and Lei Zhang. 2017. Beyond a gaussian denoiser: Residual learning of deep cnn for image denoising. *IEEE Transactions on Image Processing* 26, 7 (2017), 3142–3155.
- [80] Kai Zhang, Wangmeng Zuo, and Lei Zhang. 2018. FFDNet: Toward a fast and flexible solution for CNN-based image denoising. *IEEE Transactions on Image Processing* 27, 9 (2018), 4608–4622.
- [81] Lin Zhang, Lei Zhang, Xuanqin Mou, and David Zhang. 2011. FSIM: A feature similarity index for image quality assessment. *IEEE transactions on Image Processing* 20, 8 (2011), 2378–2386.
- [82] Shaoquan Zhang, Jun Li, Zebin Wu, and Antonio Plaza. 2018. Spatial discontinuity-weighted sparse unmixing of hyperspectral images. *IEEE Transactions on Geoscience and Remote Sensing* 56, 10 (2018), 5767–5779.
- [83] XiLe Zhao, Hao Zhang, TaiXiang Jiang, Michael K Ng, and Xiong-Jun Zhang. 2020. Fast algorithm with theoretical guarantees for constrained low-tubal-rank tensor recovery in hyperspectral images denoising. *Neurocomputing* 413 (2020), 397–409.
- [84] Yu-Bang Zheng, Ting-Zhu Huang, Xi-Le Zhao, Tai-Xiang Jiang, Teng-Yu Ji, and Tian-Hui Ma. 2020. Tensor N-tubal rank and its convex relaxation for low-rank tensor recovery. *Information Sciences* 532 (2020), 170–189.
- [85] Yu-Bang Zheng, Ting-Zhu Huang, Xi-Le Zhao, Tai-Xiang Jiang, Tian-Hui Ma, and Teng-Yu Ji. 2019. Mixed noise removal in hyperspectral image via low-fibered-rank regularization. *IEEE Transactions on Geoscience and Remote Sensing* 58, 1 (2019), 734–749.
- [86] Xizhou Zhu, Weijie Su, Lewei Lu, Bin Li, Xiaogang Wang, and Jifeng Dai. 2021. Deformable detr: Deformable transformers for end-to-end object detection. In *ICLR*.
- [87] Lina Zhuang and Jose M Bioucas-Dias. 2018. Fast hyperspectral image denoising and inpainting based on low-rank and sparse representations. *IEEE Journal of Selected Topics in Applied Earth Observations and Remote Sensing* 11, 3 (2018), 730–742.
- [88] Daniel Zoran and Yair Weiss. 2011. From learning models of natural image patches to whole image restoration. In *Proceedings of the IEEE International Conference on Computer Vision*. IEEE, 479–486.